Synthetic laihunite ($\square_x Fe^{2+}_{2-3x} Fe^{3+}_{2x} SiO_4$), an oxidation product of olivine

SHINJI KONDOH, MASAO KITAMURA, AND NOBUO MORIMOTO

Department of Geology and Mineralogy
Faculty of Science, Kyoto University, Kyoto 606, Japan

Abstract

Laihunite ($\square_x Fe^{2+}_{2-3x} Fe^{3+}_{2x} SiO_4$) has been produced by heating single crystals of synthetic fayalite ($Fe_2 SiO_4$) in the air at 400, 600, and 700°C. Opaque complexes produced at the surfaces and internal defects of the heated crystals consist of iron oxides, amorphous silica and laihunite. No laihunite has been observed in the crystals heated above 800°C.

Chemical analysis of the heated fayalite by an analytical electron microscope shows that diffusion of Fe^{2+} ions to the surfaces and internal defects took place during the oxidation process, and produced iron oxide-silica complexes. This diffusion resulted in Fe-depletion zones in fayalite surrounding the complexes. Three types of laihunite have been formed in the Fe-depletion zone. Laihunite-2M ($\square_{0.37} Fe^{2+}_{0.90} Fe^{3+}_{0.73} SiO_4$) overgrew on hematite-silica intergrowths, and laihunite-3M ($\square_{0.24} Fe^{2+}_{1.28} Fe^{3+}_{0.48} SiO_4$) in the intermediate region between laihunite-2M and fayalite. Planar precipitates of laihunite of the Guinier-Preston zone type, with thickness of about 18Å, have also been found in fayalite around laihunite-3M. The synthetic laihunites within fayalite have larger unit cells than the natural laihunite-3M ($\square_{0.4} Fe^{2+}_{0.8} Fe^{3+}_{0.8} SiO_4$) due to elastic strain.

Introduction

In order to characterize oxidized olivines and to elucidate the oxidation process of olivine, many investigations of oxidized olivines, natural and synthetic, have been carried out (Brown, 1982, p. 301). Champness and Gay (1968) and Champness (1970) investigated heated products of the forsterite-fayalite series by X-ray diffraction, infrared spectroscopy, and electron microscopy. Champness and Gay (1968) described appearance of an unidentified phase with a superstructure of olivine at an early stage of oxidation of the Fe-rich olivine and suggested it to be an "oxidized olivine". Champness (1970) reported formation of well-oriented hematite- and magnetite-like precipitates and amorphous silica by oxidation of the Fe-rich olivine at the temperature range between 500 and 800°C.

Putnis (1979) reported an "oxidized olivine" that has a superstructure of olivine in a Mg-rich cumulus olivine in the Rhum Layered Intrusion. Kohlstedt and Vander Sande (1975) found poorly identified Fe-rich "(001) planar precipitates" which resemble Guinier-Preston zones (hereafter G.P. zones), in naturally oxidized olivine in lherzolite xenoliths. However, these extensive studies have not yet been successful in elucidating the characteristics of the "oxidized olivine" or the "unidentified phase" in oxidized olivine.

On the other hand, Laihunite Research Group (1976) found a new mineral, laihunite, in an iron ore deposit in China giving the ideal chemical formula of $Fe^{2+} Fe^{3+}_2 SiO_4$. Laihunite has also been reported from volcanic rocks (Schaefer, 1983) and from druses of tuff (Matsuura et al., 1983). The structure was determined to be a distorted

olivine-type structure with $P2_1/b$ (Ferrifayalite Research Group, 1976; Fu et al., 1979). Later, Shen et al. (1982) and Li et al. (1981) reported that laihunite always shows satellite reflections along the c^* axis indicating superlattice structures of a distorted olivine type structure with a $2c$ or $3c$ repeat. Kondoh et al. (1984) have also reported an occurrence of laihunite with the basic structure of $1c$ repeat in dacite. The Ramsdell notation is used in this paper to distinguish laihunites with different superlattices, for example, laihunite-3M (laihunite-$Mab3c$) and laihunite-2M (laihunite-$Mab2c$), the notation in parentheses being the corresponding modified Gard notation (Bailey, 1978). In this paper, 2M and 3M are occasionally used for laihunite-2M and laihunite-3M, respectively, for simplicity.

Kitamura et al. (1984) studied the prototype laihunite from China by electron microscopy and reported that natural laihunite usually contains fine magnetite lamellae, inferring that the laihunite-magnetite intergrowths were derived by oxidation of fayalite. They also reported that the laihunite consists of laihunite-3M or irregular intergrowths of laihunite-2M and laihunite-3M. Tamada et al. (1983) indicated the nonstoichiometric character of laihunite-3M by deriving the chemical formula of $\square_{0.4} Fe^{2+}_{0.8} Fe^{3+}_{0.8} SiO_4$ through determination of the average structure of the laihunite-3M. Wang (1980) discussed the stability field of laihunite in the system of $Fe_2 O_3$–FeO–SiO_2, based on the thermodynamic consideration of laihunite and coexisting minerals, deriving an unrealistic stability field of laihunite.

In order to elucidate the formation process of laihunite

from fayalite and to examine the relation between laihunite and the "unidentified phase" in oxidized olivine reported in the previous studies, oxidation of olivine, especially fayalite, at atmospheric pressure has been studied in this investigation.

Experimental and results

Materials and heating

The starting material was a single crystal of pure fayalite, which was synthesized by the floating-zone method under a controlled oxygen fugacity (Takei, 1978). Thin sections of the single crystal parallel to (100) and (001) of about 30 μm thickness, were cut from the fayalite boule, whose dimension was about 12 mm long and 8 mm in diameter. They were heated on an alumina boat in a resistance furnace under atmospheric pressure, and finally cooled to room temperature. The heating temperature was fixed at 400, 600, 700, and 800°C for different samples. Heating was continued until the samples became almost opaque to light. Precipitates of opaque complexes were observed at the surfaces and cleavages parallel to (010) of the crystals under an optical microscope (Fig. 1). The total heating time was one hour at 800°C (specimen number, R-800), three hours at 700°C (R-700), five hours at 600°C (R-600), and 480 hours at 400°C (R-400). The specimen heated for 0.5 hours at 600°C (R-600S) was also prepared for comparison with R-600. In order to examine possible reaction during cooling, a specimen was studied which was quenched rapidly into liquid nitrogen after heating for 5 hours at 600°C.

X-ray study

In order to examine the phases produced by heating at different temperatures and their topotactic relations to the host, X-ray diffraction patterns of fragments of the heated specimens were taken by Weissenberg and precession methods. Hematite and magnetite are main products of fayalite in R-800. In R-700, only hematite was detected by the X-ray method. In R-600 and R-400, hematite and laihunite were main products (Fig. 2). Two kinds of satellites from laihunite appear along the c^* axis which belong to laihunite-2M and 3M.

Topotactic relationships of the iron oxides to the host fayalite have been kept constant at all temperatures with $[100]_{Fa}$ // $[001]_{Hem}$ and $[001]_{Fa}$ // $[210]_{Hem}$ for hematite, and $[100]_{Fa}$ // $[111]_{Mt}$ and $[001]_{Fa}$ // $[110]_{Mt}$ for magnetite, where Fa, Hem, and Mt represent fayalite, hematite, and magnetite, respectively. These topotactic relations are the same as those reported by Champness (1970).
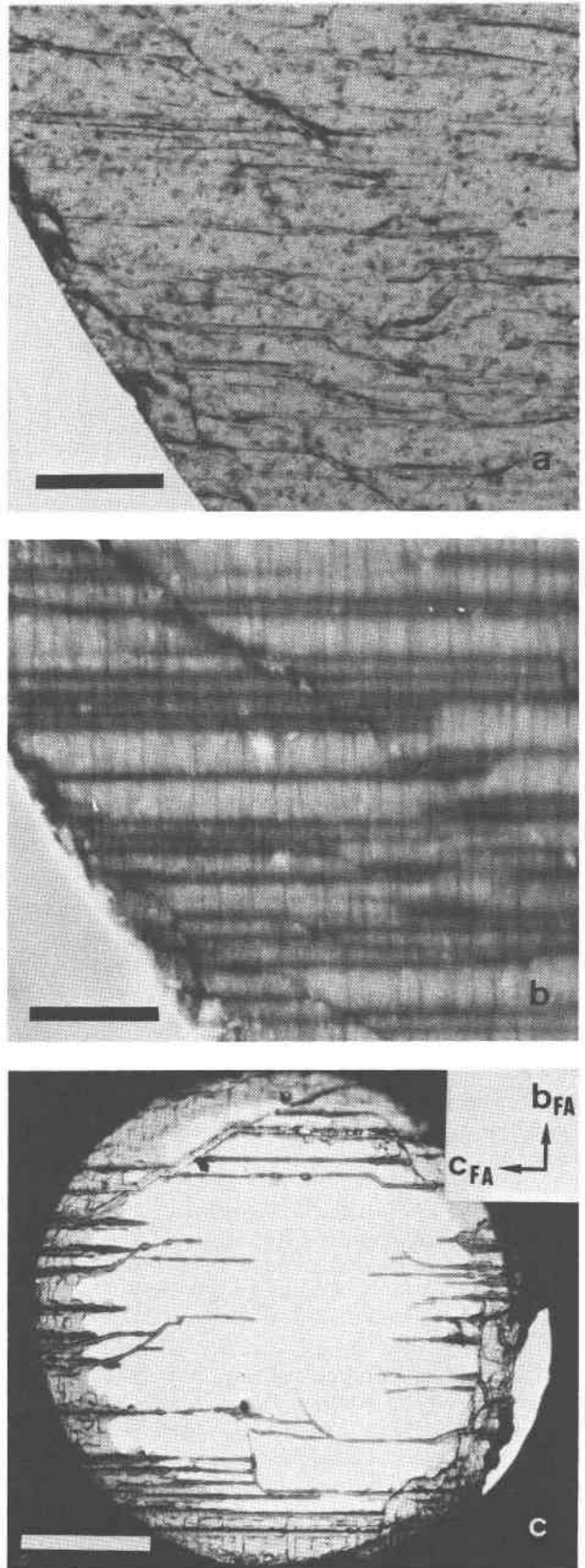
Fig. 1. Optical micrographs of a specimen (heated at 600°C) for electron microscopy. (a) Thin section of fayalite. A number of cleavages are observed parallel to (010). (b) Heated thin section. Most of cleavages were oxidized and decorated with opaque complexes. Less pronounced decoration is also observed along the defects perpendicular to (010). (c) Ion thinned specimen. Opaque complexes which decorate (010) cleavages remain as "rods". Scale bars represent 0.2 mm. The **b** and **c** axes of fayalite (FA) are indicated in (c).
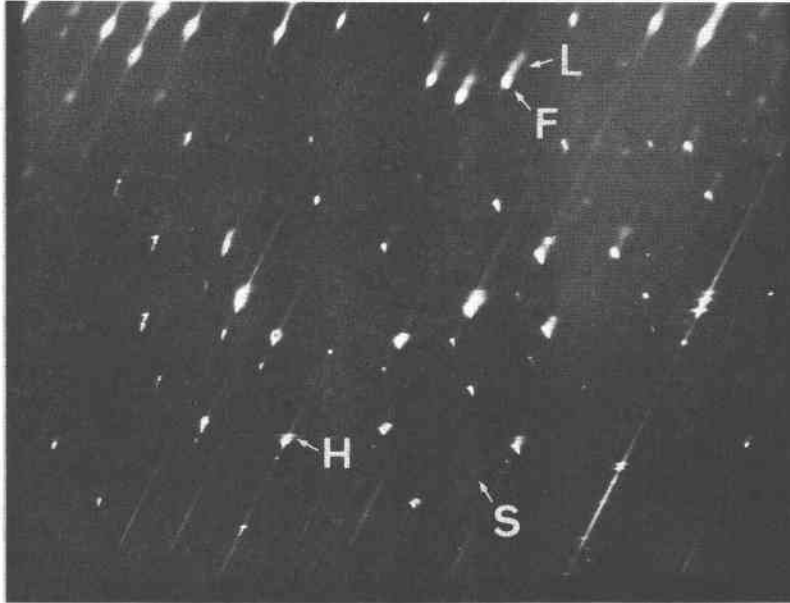
Fig. 2. Weissenberg photograph of R-600. The rotation axis is [100]. The reflections from fayalite (F), hematite (H), and laihunite (L) and the satellite from laihunite (S) are indicated.

Analytical electron microscopy

Heated thin specimens were ion-thinned for transmission electron microscopy (TEM). Because the unaltered parts of the heated thin specimen were weak to ion bombardment, only needle-like rods or prominents of a few μm in diameter with a core of opaque minerals remained from the ion-thinning (Fig. 1c). The ion-thinned specimens were studied using a high resolution 200 kV transmission electron microscope (HITACHI H-700H) with an energy dispersive X-ray analyzer (Morimoto and Kitamura, 1981).

R-800. An electron micrograph (Fig. 3) shows the opaque complexes around the cleavage face of R-800, which consist of three different regions. A band region about 2000Å in width in the central part of the complexes along the E–W direction contains hematite, magnetite, and amorphous silica (HMS zone). This HMS zone is separated from the fayalite region (F zone) by a magnetite-silica intergrowth layer (MS zone), which is the most dominant reaction product of R-800. Dark and bright lamellae in the MS zone (Fig. 3) correspond to magnetite and amorphous silica, respectively, and have a period of about 140Å. The unaltered fayalite region (F zone) in the upper part is sharply separated from the MS zone. No other phases are observed in R-800.

The ratios of the characteristic intensities of Fe and Si, I_{Fe}/I_{Si} by analytical electron microscopy (AEM) along the direction normal to the cleavage surface indicate that the Fe content becomes progressively lower in the order HMS, F, MS zone (Fig. 4).

R-600. In R-700, R-600, and R-400, the opaque complexes consist of five different regions: (1) a band-like region in the central portion with hematite, magnetite, and amorphous silica (HMS zone); (2) a region next to the HMS zone with hematite-silica intergrowth (HS zone); (3) a region with laihunite-2M and 3M (L zone); (4) a region with planar precipitates in the fayalite matrix (PF zone); and (5) an unaltered fayalite region (F zone). Because R-700, R-600, and R-400 have similar textures, the characteristics of the textures in R-600 only are described below.

A bright field electron micrograph of the opaque complexes (Fig. 5) represents common types of oxidation products in R-600. At the central portion of the complexes in the micrographs, an HMS zone of about 3000Å in width runs in the E–W direction. The central HMS zone is always surrounded by the HS zone. In some complexes, the HS zone is thin, with a thickness of about 300Å (Fig. 5). In other complexes, however, a cluster of hematite–silica intergrowths grew parallel to [010] of fayalite in the HS layer, resulting in a mushroom-like appearance at a microcrack which was possibly a dislocation-like defect. Such a mushroom-like HS-cluster is shown in Figure 8. Dark and bright contrasts in the "mushroom" represent fine hematite-silica intergrowths. Though the morphological orientation of hematite looks random, a constant topotactic relationship between hematite and host fayalite was confirmed by electron diffraction of both phases.

The clusters of hematite–silica intergrowth are wrapped by laihunite with the 2M and 3M superstructures. The interfaces between the 3M and fayalite are {023} and {001} of fayalite (Fig. 6), the former of which was described for natural laihunite by Kitamura et al. (1984). A grown "mushroom" of R-600 is usually covered by laihunite-2M which gradually changes to the 3M toward the interface between fayalite and laihunite.
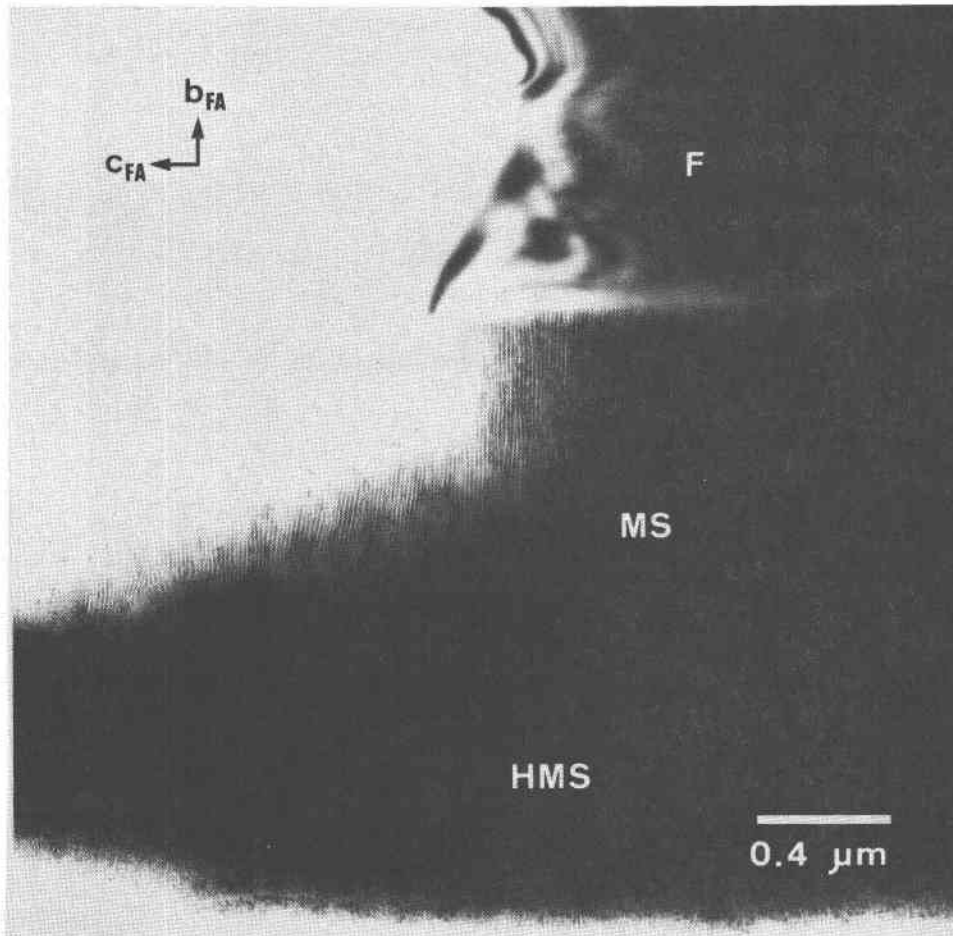
Fig. 3. Electron micrograph of an opaque complex in R-800. The "rod" along [001] of fayalite runs parallel to the E-W direction. The HMS, MS, and F zone are indicated. White region is empty. The **b** and **c** axes of fayalite (FA) are indicated.
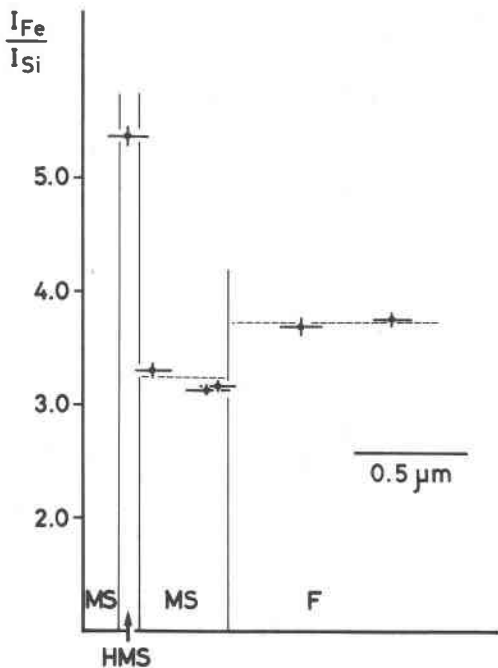
Planar precipitates parallel to {001} of fayalite are observed around laihunite and are shown as PL (Fig. 5). In enlarged micrograph (Fig. 7), they are about 18Å in thickness, suggesting a $3M$-like superstructure of laihunite. They precipitated in the fayalite matrix along the growth direction of laihunite-$3M$, and terminated so as to keep the extension of the {023} interface of fayalite with laihunite.

In another region in the PF zone in R-600, dense planar precipitates occur and show a transitional stage to a cluster of laihunite. Therefore, the planar precipitate is a G.P. zone type precipitate of laihunite, and represents an incipient stage of growth. The planar precipitates distribute over a region of several micrometers from the opaque complexes, become thinner farther away from the complexes, and finally disappear.

Because the textures of the opaque complexes in the specimens quenched into liquid nitrogen are the same as

Fig. 4. Ratios of the characteristic X-ray intensities of Si and Fe, I_{Fe}/I_{Si}, plotted perpendicular to the "rod" of the opaque complex in R-800. The boundaries between the different zones are indicated by vertical solid lines. The vertical and horizontal error bars indicate the standard deviation of the mean values and the size of the contamination spots in the analysis.
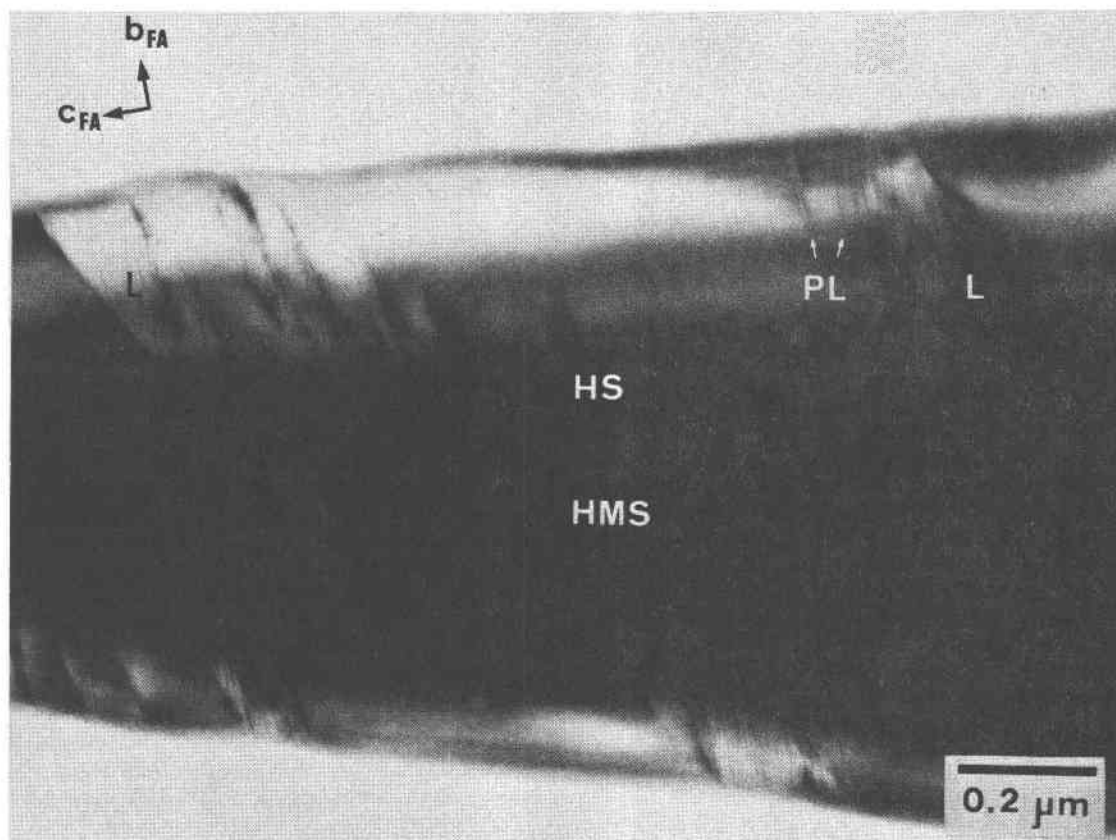
Fig. 5. Electron micrograph of an opaque complex in R-600. The complex consists of HMS, HS, L, and PF zones. The planar precipitates (PL) are scattered in the PF zone. The **b** and **c** axes of the host fayalite (FA) are indicated.

those of R-600, all the textures of R-600 are considered to have formed at higher temperature rather than during cooling.

R-600S. The early stages of oxidation reaction have been studied by means of the oxidation products in R-600S. An electron micrograph of R-600S (Fig. 8) shows the opaque complexes around a cleavage surface. The constituent zones and textures of the opaque complexes are similar to those of R-600, but the band-like region in the center, corresponding to the HMS zone in R-600, contains unaltered fayalite. Thin HS clusters are formed on the microcracks (D) which possibly originated from dislocation-like defects, and laihunite-2M is contiguous with them. Those thin HS clusters show the early stage of the growth of the "mushrooms". Separate coexistence of laihunite-2M and 3M was observed in R-600S (Fig. 9). In the center of the micrograph, a band-like HMS region of about 100Å width runs parallel to [010] of fayalite along the N-S direction. This region is connected to the larger HMS band in the center of the complexes running parallel to [001] of fayalite (Fig. 8). The interface between fayalite and 2M is indexed as {043} of fayalite, that between fayalite and 3M is {023} of fayalite, and that between 2M and 3M is {061} of fayalite, respectively. The 2M encloses the hematite-silica intergrowth and the 3M surrounds the 2M and is in contact with fayalite.

The change of the ratio of I_{Fe}/I_{Si} was determined by AEM normal to the cleavage face of R-600S (Fig. 10). The ratio is highest in the HMS zone, but lower in the L zone than in the PF zone. This indicates that Fe atoms concentrated in the HMS zone resulting in the Fe-depletion zone around it. In the Fe-depletion zone, the I_{Fe}/I_{Si} decreases with proximity to the HMS zone.

Cell parameters and compositions of laihunite

The cell parameters and volumes of the synthetic laihunite-2M and 3M in this study have been determined from the X-ray and electron diffraction patterns of R-600 and R-600S (Table 1). The difference in chemical composition between both laihunites has been estimated by AEM. Laihunite-2M is more deficient in Fe content and smaller in cell volume than laihunite-3M and fayalite (Fig. 11).

Discussion

Because the oxidation products of fayalite at 800°C are clearly different from those at between 700 and 400°C, the oxidation process at 800°C will be separately discussed from that at lower temperatures.

Oxidation process at 800°C

In R-800, the HMS, MS, and F zones occur in sequence from the center of the opaque complexes to the unaltered region. In the HMS zone, fayalite completely changed to hematite, magnetite, and amorphous silica. The Fe content
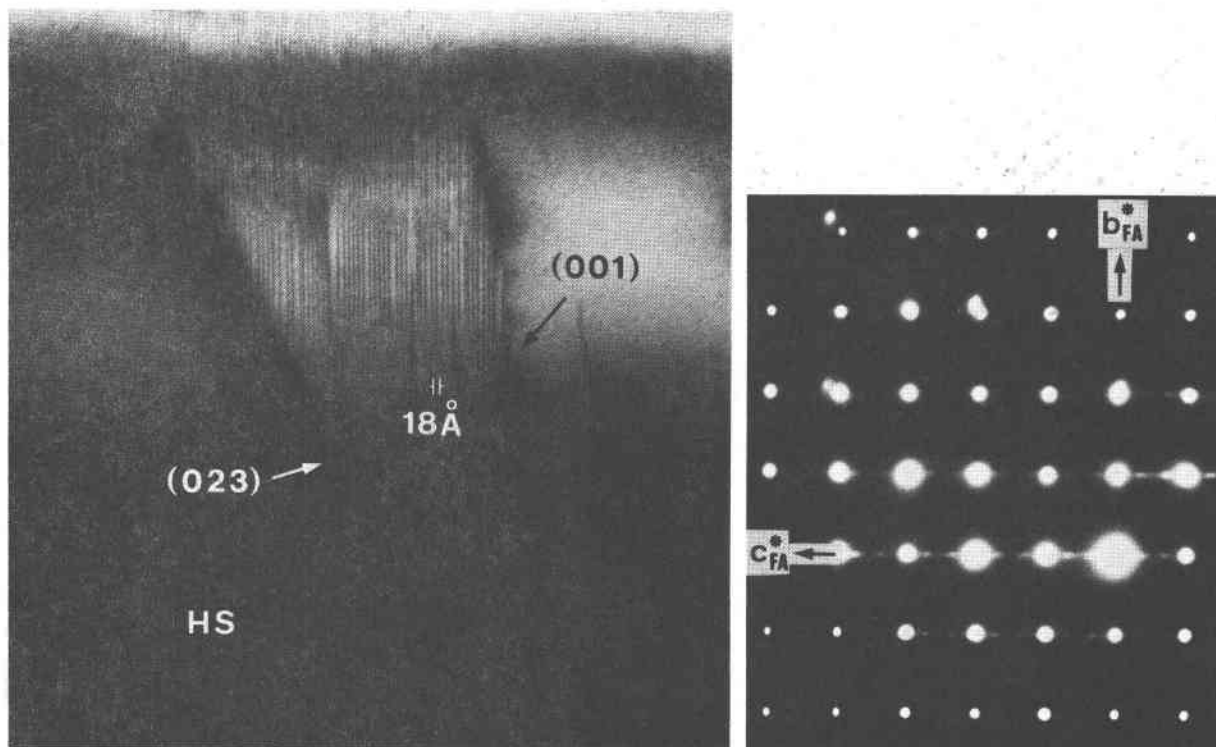
Fig. 6. High resolution electron micrograph and electron diffraction pattern of laihunite-3M in R-600. The lattice fringes of laihunite are not regular, and those of 18Å for 3M are dominant. The streaks and diffuseness of the satellites of 3M in the electron diffraction pattern reflect lack of regularity.
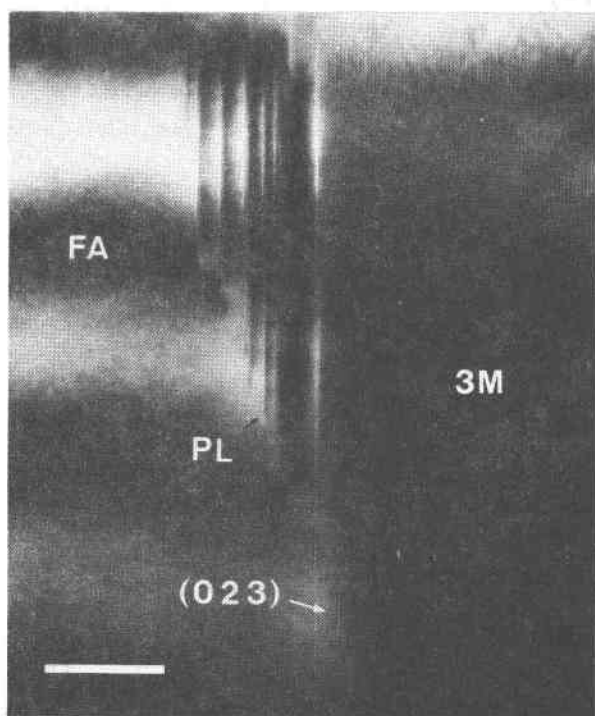
Fig. 7. Enlarged electron micrograph of planar precipitates in R-600. Planar precipitates (PL) occur in the fayalite matrix (FA) along the growth direction of laihunite-3M. Scale bar represents 500Å.

in this zone is much higher than that of other zones. The configuration of the three zones indicates a decrease of oxygen fugacity from the cleavage face (HMS zone) to unaltered fayalite (F zone). Fe^{2+} ions near the cleavage faces changed to Fe^{3+} by reaction with oxygen to form Fe_2O_3 on the cleavage surface. Fe^{2+} ions diffused to the surfaces resulting in the Fe-poor, or MS zone, around the HMS zone. If local equilibria were achieved at boundaries between the F and MS zones, and between the MS and HMS zones, their oxygen fugacities correspond to those of the FMQ and MH buffers (Lindsley, 1976, p. L-62), respectively (Fig. 12a).

The MS zone consists of regular intergrowths of magnetite and amorphous silica. Morphologic and crystallographic relations between magnetite and silica suggest the eutectoidal decomposition of fayalite through the cellular precipitation mechanism (Turnbull and Tu, 1968, p. 487; Yund and McCallister, 1970).

Oxidation process at 700, 600, and 400 °C

The HMS zone constitutes the central part of the opaque complexes as in R-800, and indicates the highest oxygen fugacity in the specimen. The thin layer of hematite–silica intergrowth, or the HS zone, is in contact with the HMS zone and is covered with laihunite.

The intergrowths of hematite and silica come directly in contact with the laihunite clusters at sharp boundaries. The texture of hematite and amorphous silica intergrowths is similar to that reported by Champness (1970) as eutectoi-
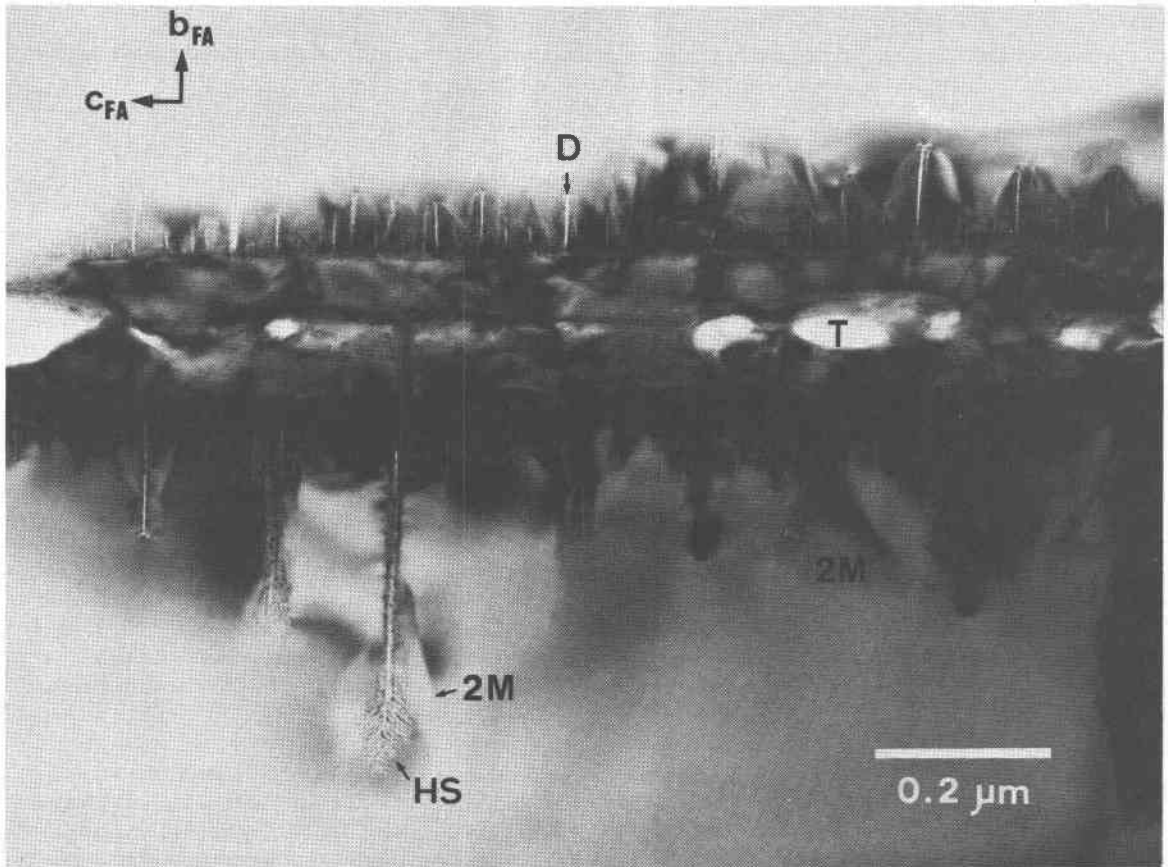
Fig. 8. Bright field electron micrograph of an opaque complex in R-600S. "Tunnel-like" holes (T) are observed in the central band-like region in the complex. The "mushrooms" of the HS cluster (HS) are identified. The clusters of laihunite-2M exist along the HS clusters. A core of the "mushroom" (D) is a microcrack which possibly originated from a dislocation-like defect.

Fig. 9. Enlarged electron micrograph of laihunite in R-600S. Laihunite-2M and 3M form a unique texture on a small crack perpendicular to the (010) cleavege of fayalite. This small crack corresponds to the fine opaque complexes perpendicular to the cleavages in Fig. 1. Reflections from fayalite (FA) and laihunite (L), and satellites of laihunite (S) are indicated in the electron diffraction pattern. The **b*** and **c*** axes of fayalite (FA) are indicated.

Table 1.   Cell parameters of laihunites, fayalite, and magnetite

		$a(\text{Å})$	$b(\text{Å})$	$c(\text{Å})$	$\alpha°$	$v(\text{Å}^3)$	$v(\text{Å}^3)*$	Source
Synthetic	2M	4.81(2)**	10.43(5)+	5.93(2)+	91.0(8)+	297(2)	18.6	Present work R-600 andR-600S
	3M	4.81(2)**	10.44(6)+	5.99(2)+	90.3(8)+	301(2)	18.8	
Natural	3M	4.805(2)	10.189(9)	5.801(1)	91.0(2)	283.9(3)	17.7	Tamada et al. (1983)
Fayalite		4.8211(5)	10.4779(7)	6.0889(5)		307.58(8)	19.22	Schwab and Kustner (1977)
Magnetite		8.396				591.9	18.49	ASTM

*   Volume for one oxygen atom.
** Measured on oscillation photographs.   The spots from the 2M and 3M could not be distinguished.
+   Determined by electron diffraction using fayalite as standard.

dal decomposition of fayalite. If the HS zone could be considered to form an independent assemblage from laihunite, the assemblage would be stable under an oxygen fugacity clearly greater than that for the HMS zone (Fig. 12). However, it is more likely that the oxygen fugacity is higher around the cleavage surface than inside the specimen as observed in R-800. Furthermore, as in Figure 8, the HS zone is always surrounded by laihunite. These observations indicate that hematite, silica, and laihunite must be considered to occur together as one assemblage under an oxygen fugacity lower than that of the MH assemblage (Fig. 12b).

The appearance of the hematite–silica–laihunite assemblage around the HMS zone below 700°C, instead of the stable magnetite–silica or magnetite–silica–fayalite assemblage, can be explained from the structural viewpoint as follows. Because the basic framework of magnetite and fayalite consists of approximately cubic and hexagonal close-packed oxygens, respectively, the decomposition of fayalite to magnetite and silica involves a drastic change in the stacking sequence of the closely packed oxygen layers, and is not likely to occur at low temperatures. Thus, the decomposition from fayalite to magnetite and silica was suppressed under the present experimental condition below 700°C.
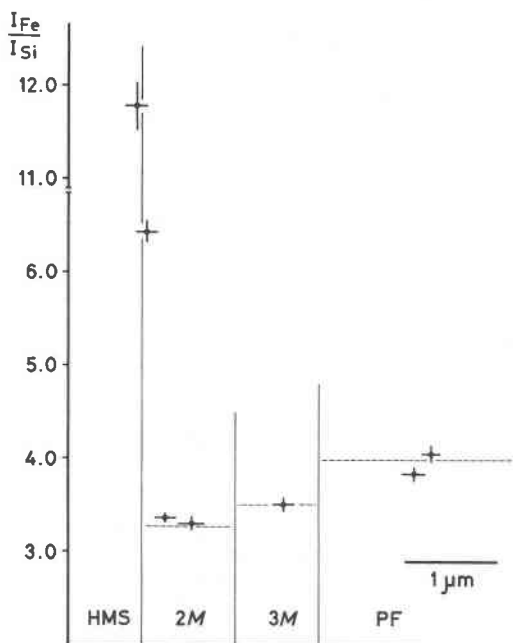
Fig. 10. Ratios of the characteristic X-ray intensities of Si and Fe, I_{Fe}/I_{Si}, along the normal to the "rod" of the opaque complex in R-600S. The boundaries between the different zones are indicated by vertical solid lines. Laihunite (L zone) is devided into 2M and 3M, which have slightly different ratios. The dashed line shows the expected level of the ratio in each zone. The vertical and horizontal error bars represent the standard deviation of the mean values and the size of the contamination spots in the analysis, respectively.
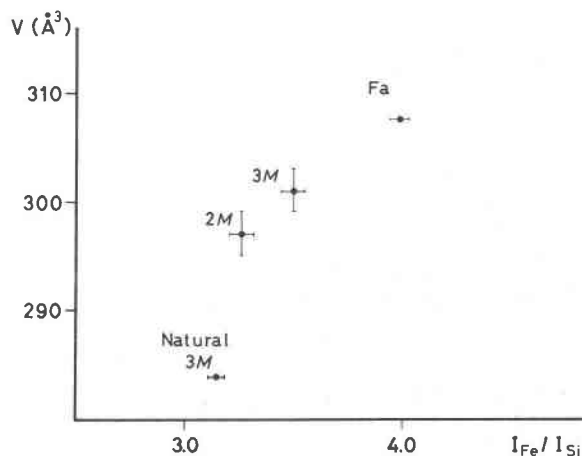
Fig. 11. Unit cell volume versus characteristic X-ray intensity ratio, I_{Fe}/I_{Si}, of synthetic laihunite-2M and 3M, natural laihunite-3M and fayalite. The error bars represent the standard deviations of the mean values. The vertical error bar of natural 3M is within the point, and the horizontal error bar is estimated by the standard deviation of the k-value (Morimoto and Kitamura, 1981). The unit cell volume of fayalite was used as standard in the estimation of the cell parameters of laihunite, and assumed to have no error.
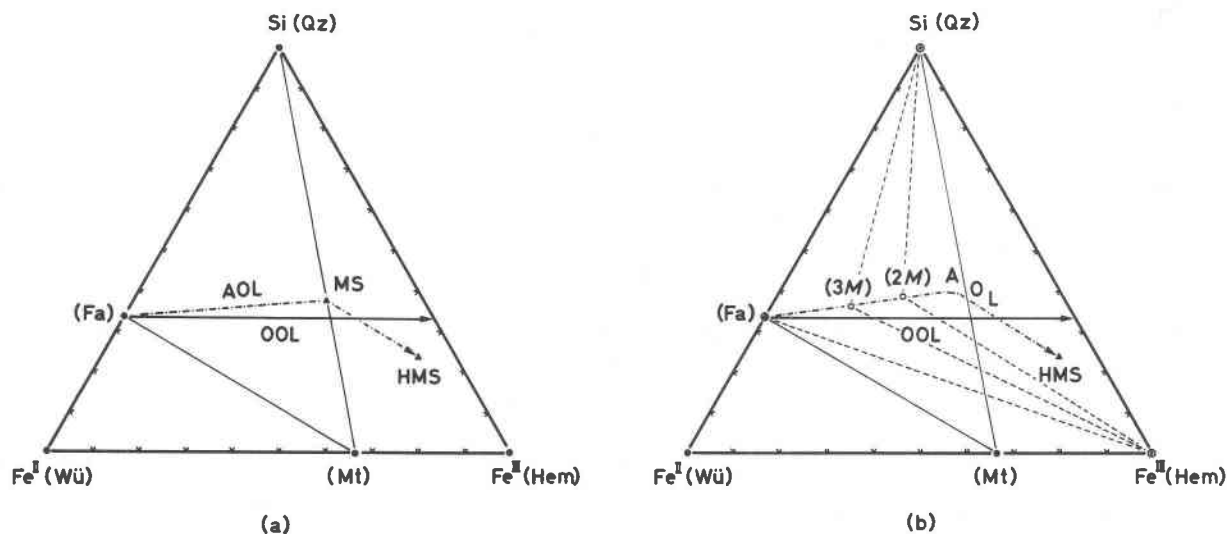
Fig. 12. Ternary FeO–Fe$_2$O$_3$–SiO$_2$ diagrams at 800°C (a) and from 700°C to 400°C (b). Fe^{II}, Fe^{III}, and Si designate the corners of the diagrams, FeO, 1/2Fe$_2$O$_3$, and SiO$_2$, respectively. The compositions of the synthetic laihunite-2M, 3M, fayalite, magnetite, hematite, and quartz are plotted. Because more Fe atoms are concentrated in the HMS zone than in fayalite and the amount of hematite is greater than that of magnetite in this zone, the bulk composition of the HMS zone is plotted near the hematite corner. The stable phase assemblages are indicated by the heavy tie lines and the phases by solid circles. The metastable phase assemblages are indicated by the dashed tie lines and the open circle phases. The ordinary oxidation process is indicated by straight heavy lines, OOL, on which the atomic ratio of Fe^{2+} + Fe^{3+} to Si is kept 2:1. In actual oxidation in this study, Fe^{2+} ions diffused to the HMS zone from the surroundings, resulting in the dot-dashed oxidation lines, AOL.

On the other hand, because fayalite, laihunite, and hematite share the framework of hexagonal close-packed oxygens, the decomposition of fayalite to laihunite, hematite, and silica is more likely at low temperature, than to magnetite and silica. Especially when the decomposition takes place in the host fayalite, the topotactic relations between fayalite and products must have a great effect on the activation energy of decomposition. Therefore, although the stable decomposition products of fayalite by oxidation around the HMS zone are magnetite and silica, a higher activation energy in the decomposition resulted in an alternative metastable assemblage of hematite, silica, and laihunite.

The configurations of laihunites-2M and 3M in the L zone are controlled by the concentration of Fe^{3+} ions. Because Fe^{3+} ions and metal vacancies are enriched in laihunite-2M relative to 3M, the 2M is usually observed along the HS zones and the 3M on the 2M in contact with fayalite. When the concentration of Fe^{3+} ions was not high enough around the HS zone, the 3M grew directly on the HS zone.

Planar precipitates, or G.P. zone type precipitates of laihunite, appear in the region of the fayalite matrix where the concentrations of Fe^{3+} ions and metal vacancies were not high enough to make the laihunite clusters. Morphology of the planar precipitates is the same as that of "(001) planar precipitates", which were observed in naturally oxidized olivine of Fo$_{92}$Fa$_8$ (Kohlstedt and Vander Sande, 1975). Champness and Gay (1968) reported unusual diffraction effects from heated olivines over a wide compositional range of the forsterite-fayalite series. They observed diffuse streaks and triplet maxima along the c* axis, which strongly suggest existence of laihunite.

Synthetic and natural laihunite

Synthetic laihunite never coexists with magnetite, but coexists with hematite and silica under the atmospheric oxidation conditions. However, natural laihunite usually coexists with magnetite. This clearly reflects differences in genetic conditions of oxygen fugacity and temperature, between synthetic and natural laihunites.

Furthermore, in the synthetic product, laihunite-2M and 3M appear as independent phases, whereas in nature the intergrowth of the 2M and 3M often appears on the scale of unit cells.

The cell volumes of the synthetic 2M and 3M, natural 3M, and fayalite are compared (Table 1). The compositions of the synthetic 2M and 3M have been obtained to be approximately $\square_{0.37}$Fe$_{0.90}^{2+}$Fe$_{0.73}^{3+}$SiO$_4$ and $\square_{0.24}$Fe$_{1.28}^{2+}$Fe$_{0.48}^{3+}$SiO$_4$, respectively, by interpolating the result of the AEM analysis between the compositions of natural 3M ($\square_{0.4}$Fe$_{0.8}^{2+}$Fe$_{0.8}^{3+}$SiO$_4$) (Tamada et al., 1983) and fayalite (Figs. 10 and 12). Large differences in cell volume between the synthetic and natural laihunites can be quantitatively explained not only by the difference in composition but also by the difference in boundary strain.

Natural 3M shows a domain texture (Kitamura et al., 1984), and the domains in contact with fayalite have a coherent interface with fayalite along {023} of fayalite. Most domains, which are far separated from fayalite, are surrounded by crystallites of magnetite with incoherent interfaces. The cell parameters of the natural 3M obtained

by the X-ray method (Tamada et al., 1983), are of the latter domains, which are free from elastic strain. In fact, the difference of the lattice translations along [0$\bar{3}$2] within (023) between fayalite and 3M caluculated from the cell parameters is much larger than that expected in the coherent interface.

On the other hand, the synthetic 3M is homogeneous and is enclosed in fayalite with coherent interfaces, {023} and {001}, which are not parallel to each other. In order to keep both interfaces coherent, the elastic strain affects the cell volume of the synthetic 3M. Thus, the strain works to keep the oxygen packing of the synthetic 3M (18.8Å^3/atom) closer to that of fayalite (19.2Å^3/atom). This results in some increase of iron in laihunite to minimize the strain energy. Therefore, the observed differences in composition and cell volumes between the natural and synthetic 3M can be explained by both elastic deformation and composition change needed for minimum total free energy. This behavior should be strongly connected with the nonstoichiometry of the laihunite.

Conclusions

Three apparently different types of laihunites have been produced by heating synthetic fayalite in air at 400, 600, and 700°C. They were distributed in the Fe-depletion region of fayalite around the hematite-silica intergrowths, which developed at surfaces and internal defects of fayalite during heating.

The three types of laihunites are laihunites-2M ($\square_{0.37}Fe^{2+}_{0.90}Fe^{3+}_{0.73}SiO_4$), laihunite-3$M$ ($\square_{0.24}Fe^{2+}_{1.28}Fe^{3+}_{0.48}SiO_4$), and planar precipitates, possibly of laihunite-3M type structure, with thickness of about 18Å. The configuration of laihunite-2M and 3M, and the planar precipitates in the Fe-depletion regions was controlled by the concentration of Fe^{3+} ions. Because Fe^{3+} ions and metal vacancies are enriched in laihunite-2M relative to 3M, 2M usually occurred on the hematite-silica intergrowths, and the 3M in the intermediate region between the laihunite-2M and fayalite. The planar precipitates appeared in the region where the concentration of Fe^{3+} ions was not high enough to form the clusters of laihunite-2M and 3M.

The synthetic laihunite-3M and 2M have larger unit cells with more iron than natural laihunite-3M. This is considered to be due to the fact that the synthetic laihunites have to keep coherent boundaries with fayalite and hematite whereas the natural laihunite is free from boundary strain.

References

Bailey, S. W. (1978) Report of the IMA-IUCr joint comittee on nomenclature. American Mineralogist, 62, 411–415.

Brown, G. E., Jr. (1982) Olivines and silicate spinels. Reviews in Mineralogy, Vol. 5, Orthosilicates. Mineralogical Society of America, Washington, D. C.

Champness, P. E. (1970) Nucleation and growth of iron oxides in olivines, (Mg,Fe)$_2$SiO$_4$. Mineralogical Magazine, 37, 790–800.

Champness, P. E. and Gay, P. (1968) Oxidation of olivine. Nature, 218, 157–158.

Ferrifayalite Research Group (1976) Ferrifayalite and its crystal structure. (in Chinese) Acta Geologica Sinica, 2, 160–175.

Fu, P., Kong, Y., and Zhang, L. (1979) Domain twinning of laihunite and refinement of its crystal structure. (in Chinese) Geochimica, 2, 103–119.

Kitamura, M., Shen, B., Banno, S., and Morimoto, N. (1984) Fine texture of laihunite. American Mineralogist, 69, 154–160.

Kohlstedt, D. L. and Vander Sande, J. B. (1975) An electron microscopy study of naturally occurring oxidation produced precipitates in iron-bearing olivines. Contributions to Mineralogy and Petrology, 53, 13–24.

Kondoh, S., Kitamura, M., and Morimoto, N. (1984) Electron microscopy of 1C-type laihunite in gas cavities in the dacite from Yugawara-cho, Kanagawa Prefecture. (abstr., in Japanese) Mineralogical Society of Japan, 1984 Annual Meeting Abstracts with program, PD-20.

Laihunite Research Group (1976) Laihunite—a new iron silicate mineral. (in Chinese) Geochimica, 2, 95–103.

Li, H., Liu, W., Kong, Y., and Fu, P. (1981) The lattice fringes of laihunite. (in Chinese) Kexue Tongbao, 10, 590–592.

Lindsley, D. H. (1976) Experimental studies of oxide minerals. Reviews in Mineralogy, Vol. 3, Oxide Minerals. Mineralogical Society of America, Washington, D. C.

Matsuura, S., Sueno, S., and Yurimoto, N. (1983) Olivine-like iron silicate mineral from Kamitaga in Shizuoka Prefecture, Japan (abstr., in Japanese). Mineralogical Society of Japan, 1983 Annual Meeting Abstracts with Program, D29, 118.

Morimoto, N. and Kitamura, M. (1981) Application of 200 kV analytical electron microscopy to the study of fine textures of minerals. Bulletin de Minéralogie, 104, 241–245.

Putnis, Andrew. (1979) Electron petrography of high-temperature oxidation in olivine from the Rhum layered intrusion. Mineralogical Magazine, 43, 293–296.

Schaefer, M. W. (1983) Measurements of iron(III)-rich fayalites. Nature, 303, 325–327.

Schwab, R. B. and Kustner, D. (1977) Präzisions-gitterkonstenbestimmung zur festlegung röntgengraphischer Bestimmungskurven für synthetische Olivine der Mischkritallreiche Forsterit-Fayalit. Neues Jahrbuch für Mineralogie, Monatshefte, 205–215.

Shen, B., Tamada, O., Kitamura, M., and Morimoto, N. (1982) The superstructure of laihunite (Fe$^{2+}_{0.5}$Fe$^{3+}_{1.0}$SiO$_4$). (in Chinese) Scientia Giologica Sinica, 3, 341–342.

Takei, H. (1978) Growth of fayalite (Fe$_2$SiO$_4$) single crystals by the floating-zone method. Journal of Crystal Growth, 43, 463–468.

Tamada, O., Shen B., and Morimoto, N. (1983) The crystal structure of laihunite ($\square_{0.4}Fe^{2+}_{0.8}Fe^{3+}_{0.8}SiO_4$). Mineralogical Journal, 11, 8, 382–391.

Turnbull, D. and Tu, K. N. (1970) The cellular and pearlitic reactions. Phase Transformations, American Society for Metals.

Yund, R. A. and McCallister, R. H. (1970) Kinetics and mechanism of exsolution. Chemical Geology, 6, 5–30.

Wang Shengyuan (1980) The stability of laihunite—a thermodynamic analysis. Geochimica, 3, 31–42.